Available online at www.sciencedirect.com
SCIENCE DIRECT
Tectonophysics 416 (2006) 289–309
TECTONOPHYSICS
www.elsevier.com/locate/tecto

Imaging global chemical and thermal heterogeneity in the subcontinental lithospheric mantle with garnets and xenoliths: Geophysical implications

S.Y. O'Reilly [a,*], W.L. Griffin [a,b]

[a] GEMOC National Key Centre, Macquarie University, NSW 2109, Australia
[b] CSIRO Exploration and Mining, North Ryde, NSW 2113, Australia

Accepted 28 November 2005
Available online 7 February 2006

Abstract

Suites of mantle-derived xenoliths in volcanic rocks provide estimates of the geothermal gradient and composition of the subcontinental lithospheric mantle (SCLM) at the time of the volcanic eruption. The development of single-grain thermometry and barometry, applied to xenocryst minerals in volcanic rocks, has greatly expanded the number of localities for which such data can be obtained and made it feasible to map the geology of the SCLM on a broader scale, both vertically and laterally. From garnet xenocrysts, it is possible to derive profiles showing mean values of olivine composition, bulk-rock composition, density and seismic velocities, as well as geotherm parameters and constraints on the thickness of the SCLM. Geochemical profiles, coupled with Re–Os dating of peridotites and their enclosed sulfide minerals, show that Archean or Proterozoic SCLM is preserved at shallow levels beneath many areas of younger tectonothermal age; this implies rapid vertical variations in Vs and Vp with depth, which may affect seismic interpretations. Data from several hundred localities worldwide define a secular evolution in the composition of the SCLM, related to the tectonothermal age of the overlying crust. Archean SCLM is typically strongly depleted in basaltic components, highly magnesian and thick (160–250 km), and has low geotherms; Phanerozoic SCLM is typically fertile (rich in basaltic components), Fe-rich, thin (50–100 km) and has a range of high geotherms; Proterozoic SCLM (much of which may be reworked Archean mantle) tends to be intermediate in all respects. The correlated variations in SCLM fertility, lithospheric thickness and geotherm reinforce the effects of each on seismic velocity, and produce more rapid lateral variations in seismic response than would result from thermal effects alone. These correlations are the key to using seismic tomography images to map the lateral extent of different types of SCLM.

Keywords: Geotherms; Lithosphere mapping; Subcontinental lithospheric mantle; Mantle heterogeneity; Mantle geophysical properties

1. Introduction

Geophysical data are yielding increasingly more detailed information on the physical properties of the lithosphere (and below). Seismic data show lateral and vertical contrasts in the density and elastic properties of the subcontinental lithospheric mantle (SCLM) (e.g. Bostock, 1999; Thybo, 2002; Snyder et al., 2003, 2004); electromagnetic responses are revealing highly conductive regions (e.g. Jones et al., 2001); integrated modelling of gravity and topography shows variations in elastic thickness for different lithosphere columns

* Corresponding author.
E-mail address: soreilly@els.mq.edu.au (S.Y. O'Reilly).

0040-1951/$ - see front matter © 2006 Elsevier B.V. All rights reserved.
doi:10.1016/j.tecto.2005.11.014

that reflect rheological variability including possible shear zones (e.g. Poudjom Djomani et al., 2003); cumulative density profiles show intrinsic differences in lithosphere columns of different ages (e.g. Poudjom Djomani et al., 2001; O'Reilly et al., 2001); very recent work suggests deep-seated lithospheric rocks may sustain intrinsic magnetic properties (Robinson et al., 2002; McEnroe et al., 2004) relevant to interpreting long-wave magnetic signals.

Geological mapping of the mantle using mantle-derived materials has now progressed to the stage where detailed geochemical imaging of significant regions of the subcontinental lithospheric mantle is possible. In particular, the use of single-grain (dominantly garnet) thermometry and barometry has enabled the vertical and horizontal mapping of lithosphere composition and rock-type distribution to a degree far beyond that accessible by mantle xenolith data and has resulted in significant advances in understanding lithosphere evolution and architecture on scales of tens of kilometres. Recent advances in in situ analysis of trace elements in minerals by laser-ablation ICPMS have made this single-grain methodology generally accessible. This paper is a review of the current knowledge of the petrological and geochemical nature of the lithospheric mantle generated using this approach, and how this can be used to interpret geophysical datasets with geological ground-truthing.

1.1. What is subcontinental lithospheric mantle?

The subcontinental lithospheric mantle (SCLM) forms the lowermost part of the lithospheric plate complex that moves in a relatively rigid way over the hotter and rheologically weaker asthenosphere. Lithosphere is non-convecting and thus characterised by conductive (or locally advective) geotherms (e.g. McKenzie and Bickle, 1988; Fig. 1). Lithosphere thickness tends to vary with tectonothermal age, so that most Archean lithosphere is thicker and cooler (today) than Phanerozoic lithosphere.

Lithospheric mantle has formed by differentiation of the primitive mantle that was residual after core formation. The main mechanisms of formation of SCLM domains include: (i) direct partial melting residues that remain after mafic melts formed in the shallow asthenosphere and migrated upwards to create, or add to, crustal material; (ii) simple cooling and upwelling of asthenosphere (e.g. at rifts and some continental margins), with resultant underplating of pre-existing lithosphere; (iii) cooling and accretion of the uppermost sections of plumes, which may be compositionally

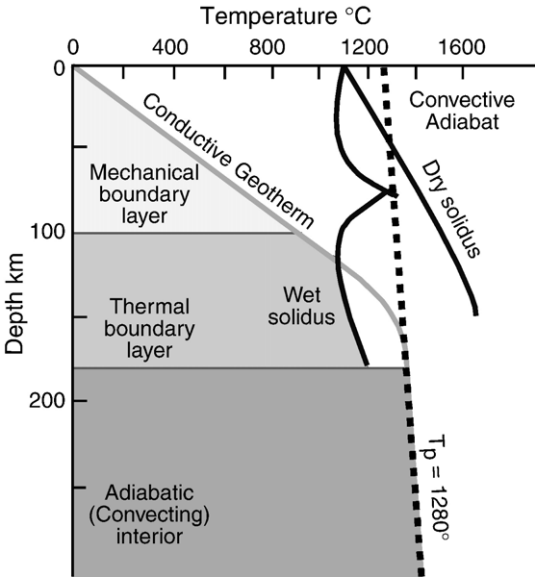

Fig. 1. Depth profile showing the lithosphere (with conductive geotherm) and the asthenosphere (with adiabatic geotherm), modified from McKenzie and Bickle (1988) and Menzies (1990). The intersection of the conductive geotherm with the wet solidus of peridotite may mark the division of the lithosphere into an upper mechanical boundary layer and a lower thermal boundary layer, which though weaker still sustains a conductive geotherm.

complex and include depleted residues, primary cooled plume components and indigenous mafic melts. Other possible, though less likely, mechanisms of forming or adding lithospheric material include crystallisation from a primordial magma ocean in the Archean (e.g. Ito et al., 2004 and references therein) and subduction of oceanic crust terranes beneath the base of pre-existing lithosphere (e.g. Helmstaedt and Gurney, 1995).

The lithosphere is geochemically distinct from the convecting mantle; it is relatively depleted in basaltic components, measured by lower Al, Ca, Fe and the abundances of specific incompatible minor and trace elements (e.g. light rare-earth elements, Ti, Zr, Y) and reflecting its residual character after the extraction of mafic melts. The degree of depletion is highly variable, ranging from very low where cooled asthenosphere forms new underplated layers that have lost little melt ("fertile") to extreme where high degrees of melting have formed highly "depleted" peridotites very low in Al, Ca and Fe, such as harzburgites (olivine and orthopyroxene rocks with no clinopyroxene). Thus, newly formed lithosphere is heterogeneous from place to place, depending on its mechanism of formation and the degree of partial melting of the primitive protolith. In addition, there is a secular evolution to less-depleted compositions for newly formed lithosphere with decreasing age, probably related to concomitant decreases

in mantle temperatures, and hence a lower potential for high degrees of mantle melting, over Earth's geological history.

Because it is non-convecting, subcontinental lithospheric mantle does not mix and homogenise, and therefore carries a geochemical, thermal and chronological record of large-scale tectonic events that involve fluid movement from the asthenosphere. SCLM domains have been overprinted by metasomatic processes since their formation and therefore are geochemically complex.

In summary, "old" lithosphere is relatively thick, highly depleted and relatively cool (at the present day), while "young" lithosphere is relatively thin, fertile and relatively hot; all SCLM has undergone some metasomatic modification since its stabilisation. The complex development of the SCLM through time has resulted in significant vertical and lateral contrasts in the compositions and geothermal profiles (and hence physical properties) of mantle domains and these must be mapped and incorporated into geophysical interpretations to develop geologically realistic models of lithosphere architecture.

To simplify the assessment of the temporal variation in lithosphere composition, we use a modified version of Janse's (1994) classification of crustal regions, which is based on tectonothermal age (the last period of major thermal perturbation). In our terminology, *Archons* experienced their last major tectonothermal event more than 2.5 Ga ago, *Protons* between 2.5 and 1.0 Ga, and *Tectons* less than 1.0 Ga (see Griffin et al., 1998b).

1.2. Lithosphere–asthenosphere boundary (LAB)

The base of the SCLM is the lithosphere–asthenosphere boundary (LAB), which is recognisable geochemically, seismically and rheologically (e.g. Wyllie, 1988; McKenzie and Bickle, 1988; Anderson, 1989; O'Reilly and Griffin, 1996; Pavlenkova, 1997) . Geochemically, the LAB is marked by the change from depleted SCLM to fertile asthenospheric compositions. Seismically, the LAB may be marked by a low-velocity zone, which is most evident in tectonically young regions and is ascribed to changes in rheology and the presence of low degrees of partial melting in that region. This low-velocity zone commonly is not detectable in old regions, although the Lehman discontinuity (Anderson, 1989; Gung et al., 2003) coincides with the geochemical LAB in some cratonic regions (Griffin et al., 1999a). Rheologically, the LAB has been interpreted as the base of the SCLM where it acts as a mechanical boundary layer (McKenzie and Bickle, 1988; Fig. 1). The temperature at the LAB is typically about 1200–1300 °C and, as the asthenosphere is convective, its geothermal gradient is generally adiabatic

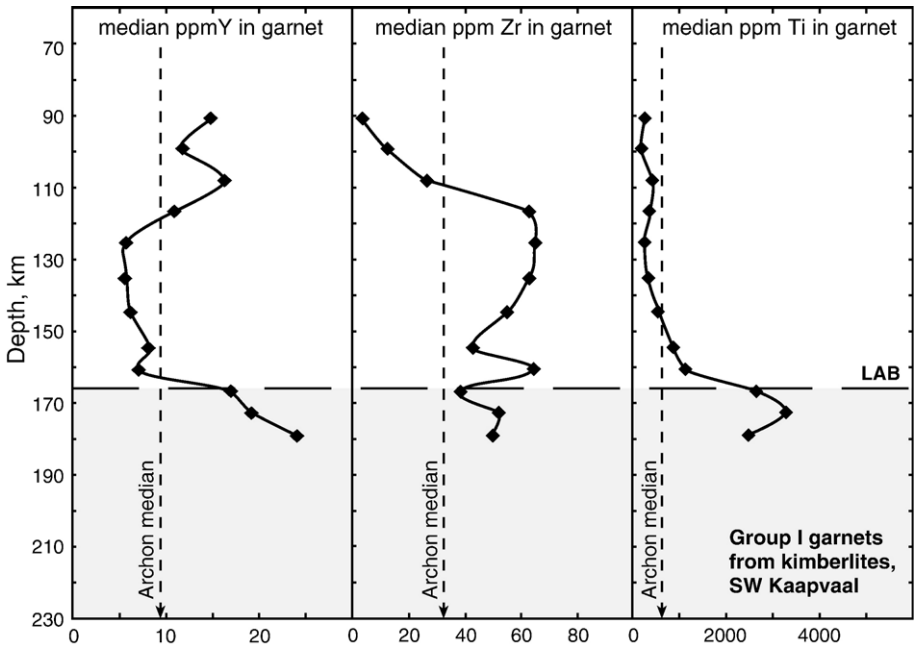

Fig. 2. Depth profiles of the concentrations of three key trace elements in peridotitic Cr-pyrope garnets from the lithosphere beneath the SW part of the Kaapvaal Craton, as sampled by Group I kimberlites (≤90 Ma eruption ages). The median values for Archon garnets worldwide are shown by the dashed lines. The enrichment in Y, Zr and Ti at the LAB reflects melt-related metasomatism, while the enrichment in Zr, but not Ti, higher in the section the section (110–150 km) suggests another metasomatic process.

(although perturbations occur due to advection of melts and fluids, geochemical reactions and melt production from transient thermal instabilities, e.g. Wyllie, 1988; Finnerty and Boyd, 1987). At the lithosphere–asthenosphere boundary, the temperatures of the lowest lithosphere and the uppermost asthenosphere must coincide, so the greater rigidity of the lithosphere is an important factor in maintaining its mechanical integrity during plate movement.

The processes of depletion that have produced the SCLM leave a characteristic geochemical pattern in key phases such as the Cr-pyrope garnets of mantle peridotites; these typically have low abundances of elements such as Y, Zr and Ti (Griffin et al., 1999c, 2002). The lowermost part of the SCLM is a chemically active region interfacing with the fertile, adiabatic, convecting mantle that continually yields small-volume melts, highly charged with incompatible elements (those which are preferentially partitioned into the melt and thus depleted from the mantle residue). These fluids strongly metasomatise the base of the SCLM, changing the compositions of the constituent minerals to produce distinctive trace-element signatures in garnets and other phases from the lowermost SCLM. Garnets in the SCLM typically have low abundances of elements such as Ti, Zr and Y, but asthenospheric small-volume melts are strongly enriched in these elements and impart this signature metasomatically to garnets around the LAB. Thus depth profiles (see below) of element distribution in mantle garnets can be used to recognise the depth extent of the depleted lithosphere and to define the LAB chemically (Fig. 2).

2. 4-D lithosphere mapping

4-D lithosphere mapping (O'Reilly and Griffin, 1996; O'Reilly et al., 2001) is an integrated methodology that uses mantle materials, geophysical datasets and geodynamic modelling to define the composition and architecture of the SCLM and trace its evolution. The fourth dimension is time, represented by the age of the host volcanic rocks that have transported the mantle material to the surface. Eruptions of volcanic rocks at different times can track changes in the lithosphere in the same location. For example, the Ordovician kimberlites and Tertiary basalts in eastern China contain mantle xenocrysts and xenoliths that demonstrate the change from typical thick, cool depleted Archean lithospheric mantle to thin, fertile, hot Phanerozoic mantle in that region (Griffin et al., 1998a).

Mantle materials include fragments of mantle rock types (xenoliths) and xenocrysts (single grains derived by disaggregation of xenoliths) entrained in ascending magmas and tectonically emplaced mantle fragments. Geophysical datasets include seismic reflection, refraction and tomography, gravity, electromagnetic and thermal information. The specific information on mantle rock types, their spatial relationships and distribution provides the basis for realistic interpretation of the geophysical datasets, and potentially allows accurate geological mapping of the SCLM globally. Conversely, as the mantle xenolith and xenocryst data provide information for point sources (virtual drill-holes), characterisation of physical properties (e.g. density, elastic properties, ambient source pressure and temperature). Recognition of the geophysical signals generated by specific rock types in specific physical environments is required to allow extrapolation of SCLM geology between these sampled sections using the geophysical (currently mainly seismic) information.

One of the key parameters in such extrapolations is the remotely sensed seismic velocity, for both compressional (Vp) and shear waves (Vs). In order to interpret seismic wave velocities meaningfully or to calculate them for different mantle domains, it is necessary to know the average whole-rock composition, the mode (proportions and type of minerals), the pressure and temperature and the spatial distribution of the relevant rock types.

The key goals in the use of mantle materials in 4-D lithosphere mapping are: determining the lithospheric paleogeotherm at the time of eruption of the host magma (a time dimension), establishing the composition of different mantle domains (vertically and laterally), dating the time of stabilisation of different mantle domains, establishing the timing and nature of important fluid-related (metasomatic) events that may reflect important large-scale tectonic episodes, and unravelling the response to important crustal events recorded in the SCLM.

2.1. Paleogeotherms

Paleogeotherms provide the framework for establishing the vertical distribution of both mantle rock types and metasomatic facies, as well as information about the thermal state of the lithosphere in timeslices defined by the age of the host volcanic eruption. Numerous thermobarometric studies of mantle-derived xenoliths have shown that in most areas, it is possible to construct a geotherm relating temperature to depth using relevant mineral equilibria in mantle-derived xenoliths (e.g. O'Reilly and Griffin, 1985; Xu et al., 1996, 1998; Smith, 1999; and references therein). Many

xenoliths have mineral assemblages that allow calculation of temperature but are unsuitable for calculating pressure. If a robust geotherm can be established for a given region, then temperatures of such xenoliths can be referred to the geotherm and a depth (pressure) can be estimated.

2.1.1. Xenocryst geotherms

Suitable xenolith suites are limited in their geographic and temporal distribution, and assembling statistically representative databases using xenolith geothermobarometry is too time-consuming to be feasible on a global scale. Xenocrysts, especially garnet and chromite, are much more abundant (and more resistant to alteration than the other dominant mantle minerals, olivine and pyroxene) and can be analysed rapidly in grain mounts; therefore, the development of robust thermometers based on single-element partitioning (Ni in Cr-pyrope garnets, Zn in chromite) with mantle olivine was an early goal of our 4-D lithosphere mapping (O'Reilly and Griffin, 1996; Ryan et al., 1996).

Cr-pyrope garnets disaggregated from mantle peridotites are in equilibrium with mantle olivine, which shows a very narrow range of Ni content (about 3000 ppm), and this allows the calculation of garnet-olivine equilibration temperature (T_{Ni}) from the measured Ni in the garnet (Griffin et al., 1989; Ryan et al., 1996). This temperature can then be referred to a known geotherm to determine pressure. In addition, if the Cr-pyrope is in equilibrium with chromite in the peridotite, then the Cr content can be used as a geobarometer (Fig. 3; Ryan et al., 1996). It is important to note that mantle-derived eclogitic garnets cannot be used in this way, as they have not been in equilibrium with olivine. Such eclogitic garnets typically have less than 1% Cr_2O_3, commonly lower Mg# than peridotitic garnets, and may have higher CaO contents than peridotitic garnets.

The construction of a garnet geotherm is illustrated in Fig. 2 where calculated T_{Ni} and P_{Cr} values are plotted in T–P space. Cr-saturated garnets will define a locus of maximum P_{Cr} at any T_{Ni}, and this locus is taken as the geotherm; the P_{Cr} estimates for these garnets give a realistic estimate of their depth of origin. Garnets that are not Cr-saturated (have not equilibrated with chromite) are recognised empirically as they scatter in the low-pressure region away from the locus of maximum P_{Cr}, as shown in Fig. 2, and provide no true P estimate. These garnets that did not equilibrate with chromite will give minimum P_{Cr} estimates, but their depth of origin can be derived by extrapolating along a constant-temperature line to the garnet-derived geotherm (Fig. 3). The Zn content of mantle chromites (in equilibrium with peridotitic olivine) can also be used to estimate T (Ryan et al., 1996) and histograms showing the distribution of temperatures for suites of chromite grains can show the vertical distribution of chromite in the mantle (by reference to the garnet geotherm), providing a cross-check on the inferred distribution of Cr-saturated garnets.

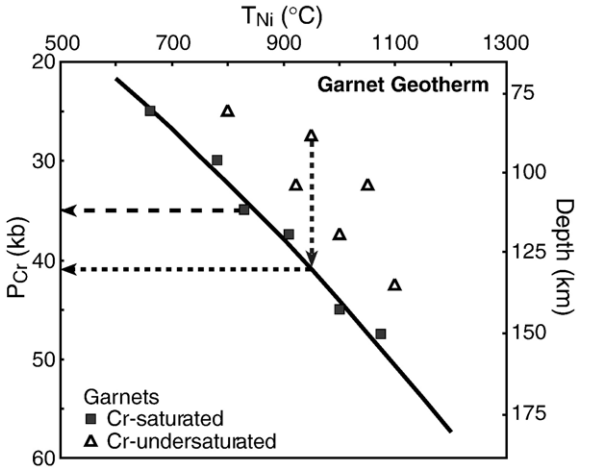

Fig. 3. Schematic showing the derivation of a garnet geotherm from a group of garnet analyses, as the locus of points through the highest P_{Cr} at each T_{Ni}, defined by Cr-saturated garnets. Garnets undersaturated in Cr will give minimum P estimates, but their depth of origin can be estimated by projecting their T_{Ni} to the geotherm (dotted line).

This single-element partitioning approach has proved to be an invaluable methodology that allows the use of the relatively abundant disaggregated xenocrysts to derive geotherm parameters from suites of garnet and spinel xenocrysts and thus allows each garnet xenocryst to be restored to its original depth context, as well as defining the mantle thermal environment. Where suites of both xenoliths and xenocrysts are available, the two approaches give concordant results (e.g. Ryan et al., 1996) validating this approach.

The xenolith/xenocryst geotherm for Group I kimberlites in the SW part of the Kaapvaal Craton (Fig. 4a) lies between the 35 and 40 mW/m^2 model conductive geotherms (Pollack and Chapman, 1977) and slightly below the xenolith-derived geotherm (Fig. 4b), which approximates a 40 mW/m^2 geotherm. A plot of Y in garnet against temperature (Fig. 4c) shows that depleted garnets (typical of the SCLM) do not occur above ca. 1100°C. We take this temperature as defining the geochemical LAB; it corresponds to a depth of about 170 km by reference to the geotherm. We assume this is the depth limit of the conductive geotherm; below this depth, the "perturbed" part of the geotherm is

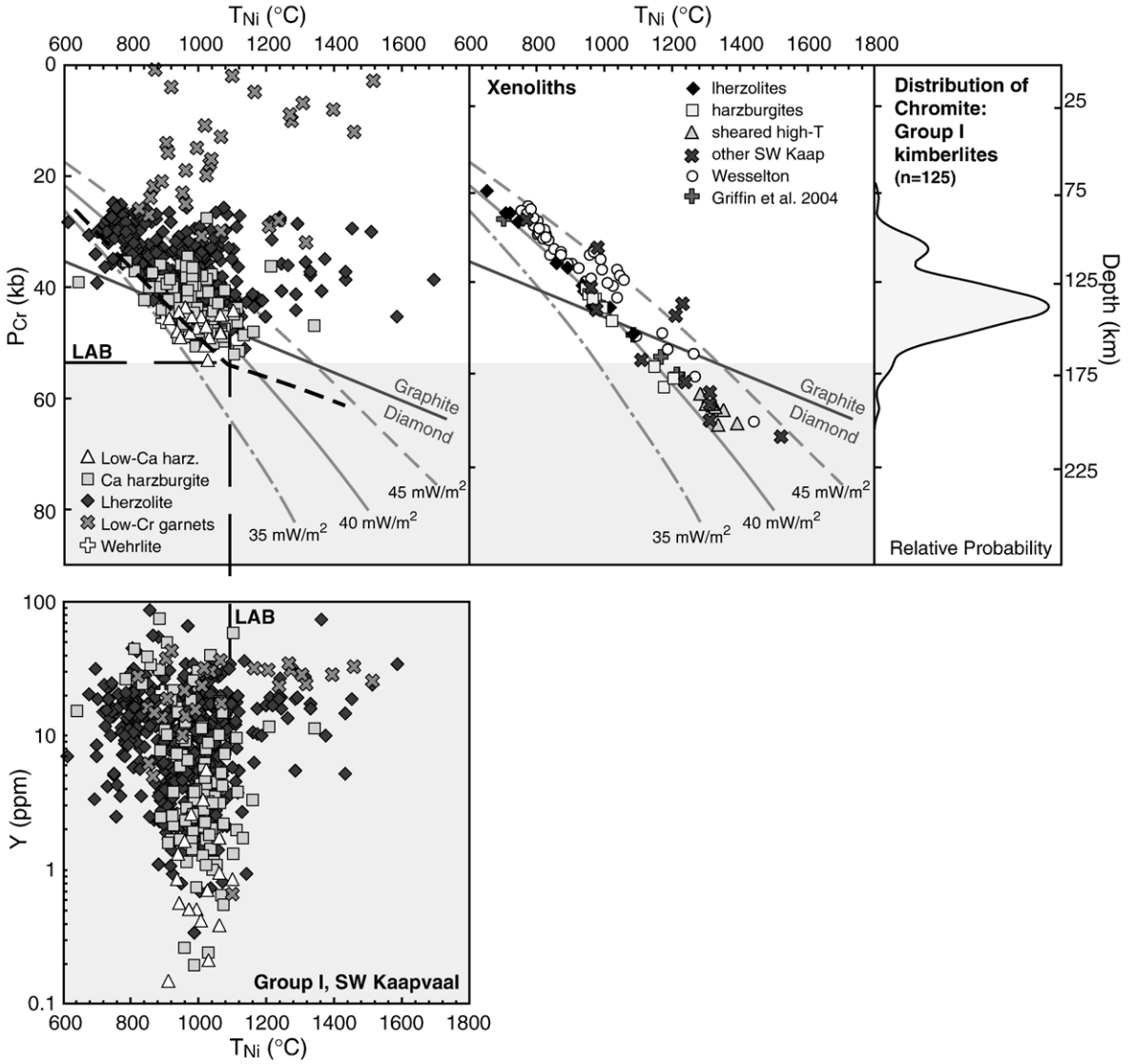

Fig. 4. Geotherm and LAB data for Group I kimberlites, SW Kaapvaal Craton. (a) T_{Ni}–P_{Cr} data for peridotitic garnets from heavy-mineral concentrates, showing a garnet geotherm corresponding to a 38 mW/m^2 conductive model geotherm (light dashed line); (b) P–T estimates (ONW T, NG P) for peridotite xenoliths, with data from James et al. (2004) and authors' database; (c) depth distribution of chromites, based on T_{Zn} estimates referred to the garnet geotherm, shows that Cr-saturated garnets are unlikely to be present below 165 km depth; (d) Y contents of peridotitic garnets (legend as in (a)) vs. T_{Ni}; depleted garnets are rare at $T>1100$ °C, corresponding to a depth of 165 km, and this is taken as the LAB (thick dashed line).

drawn parallel to the diamond-graphite curve, because the only constraint is provided by the *PT* relationships of high-temperature sheared peridotites, which scatter about this locus (e.g. Finnerty and Boyd, 1987). This depth also marks a drop in the abundance of chromite, which is reflected in the relatively low calculated P_{Cr} for garnets with $T_{Ni}>1100$ °C (Fig. 4d). The sheared xenoliths signal a perturbed thermal state interpreted as due to the infiltration of high temperature, small-volume (asthenospheric) fluids into the lowermost lithospheric mantle, coinciding with the change in garnet compositions from typical depleted "lithospheric" to enriched signatures. This infiltration is generally considered to have occurred immediately before the xenoliths were entrained (e.g. Griffin et al., 1996) as this thermal perturbation is transient. The geochemical fingerprint of this event allows us to define the geochemical lithosphere–asthenosphere boundary by the downward increase in Y (and other incompatible elements) content as described above.

Many of the xenolith- and xenocryst-derived geotherms approximate models of conductive heat transport; the deviations caused by local thermal effects (such as magma conduits) are relatively small and leave distinctive geochemical fingerprints that allow their recognition. We have constructed empirically, or compiled from published data, xenolith/xenocryst paleogeotherms for over 300 localities worldwide. These xenolith/xenocryst-based paleogeotherms are typically low (at the present day) beneath cratonic areas with Archean crust, higher beneath Proterozoic cratons and still higher beneath Phanerozoic mobile belts (Fig. 5). In areas of active basaltic volcanism, such as eastern Australia and eastern China (O'Reilly and Griffin, 1996; O'Reilly et al., 2001), xenoliths and xenocrysts in the basalts generally record high, strongly upward-convex geotherms, consistent with advective heat transport by magmas and underplating of basaltic rocks in the upper part of the lithospheric mantle (e.g. Griffin and O'Reilly, 1987; O'Reilly et al., 1997; Cull et al., 1991). These empirical geotherms reflect covarying temperatures and pressures measured with depth in specific mantle sections. Surface heat-flow values have been used (e.g. Pollack and Chapman, 1977; Nyblade, 1999) to extrapolate temperatures downward, giving model geotherms that serve as useful reference curves.

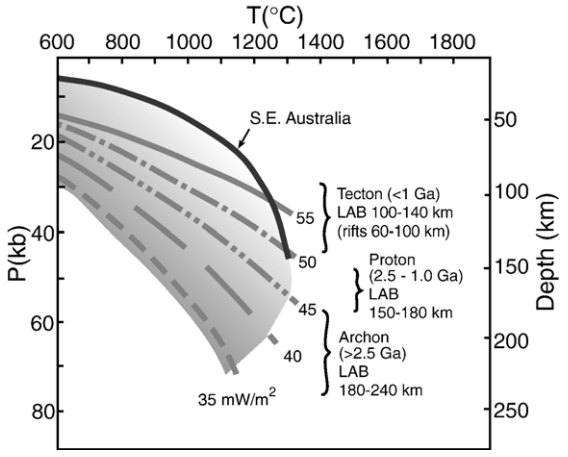

Fig. 5. Summary of typical xenolith-based geotherms and LAB depths for Archon, Proton and Tecton settings. The geotherms are empirically constructed as described in the text, by plotting the calculated pressure and temperature of equilibration of each xenolith in pressure–temperature space. These geotherms are thus model-independent and do not rely on extrapolation of surface heat flow data with the attendant problems of estimating heat production and thermal conductivity of different lithosphere regions (as discussed in O'Reilly and Griffin, 1985; O'Reilly et al., 1997). The SE Australia geotherm (O'Reilly and Griffin, 1985) is typical of many regions of young intraplate magmatism and reflects advective heat transport by magmas, typically underplating near the crust–mantle boundary.

However, such models are intrinsically limited because poorly constrained parameters such as thermal conductivity and radiogenic heat production are variable both with depth and laterally in continental crust, and in the SCLM.

The empirically constructed xenolith-derived geotherms are independent of the uncertainties of model geotherms. The xenolith-derived geotherms are constructed by the calculation of the pressure (P) and temperature (T) of equilibration of about 20–30 individual mantle xenoliths from a particular volcanic that samples the underlying mantle. Where a sufficient depth range of that mantle has been sampled, the locus of those P and T points defines the geotherm for that mantle section at the time it was sampled (O'Reilly and Griffin, 1985). This method uses mineral geothermometers and geobarometers based on T- and P-dependent element partitioning between mantle minerals, rigorously tested experimentally and thermodynamically (e.g. Smith, 1999 and references therein). The garnet geotherms are constructed analogously as described above, using populations of single garnet grains, also independent of any assumptions about variables such as thermal conductivity, heat production and heat exchange mechanisms.

2.2. Calculation of olivine composition using garnet xenocrysts

Olivine is the most abundant mineral in the SCLM and the X_{Mg} (Mg/(Fe+Mg)) of olivine is important in controlling the physical properties of lithospheric regions (density, Vp, Vs; Poudjom Djomani et al., 2001; O'Reilly et al., 2001). Olivine does not obey Birch's law (e.g. Birch, 1961) in which increasing seismic velocity correlates with higher density. Mg-rich olivine (e.g. $Fo_{92–94}$, typical of depleted mantle regions) has lower density but higher seismic velocity than Fe-rich olivine (e.g. $Fo_{88–90}$, typical of more fertile mantle regions). A change in the forsterite content of olivine by 1% (=$0.01X_{Mg}$) changes its density by 0.3% and its mean Vs by 0.22% (Anderson and Isaak, 1995).

Because olivine is more rarely preserved than garnet xenocrysts and does not contain information that defines its depth of origin, an inversion of the garnet-olivine Fe–Mg exchange geothermometer of O'Neill and Wood (1979) was developed to calculate the X_{Mg} of olivine coexisting with garnet grains (Gaul et al., 2000). This allows the vertical profile of olivine composition (Fig. 6) in any section sampled by garnet xenocrysts to be plotted using the T_{Ni} of garnet and the geotherm. X_{mg} generally shows a distinct decrease

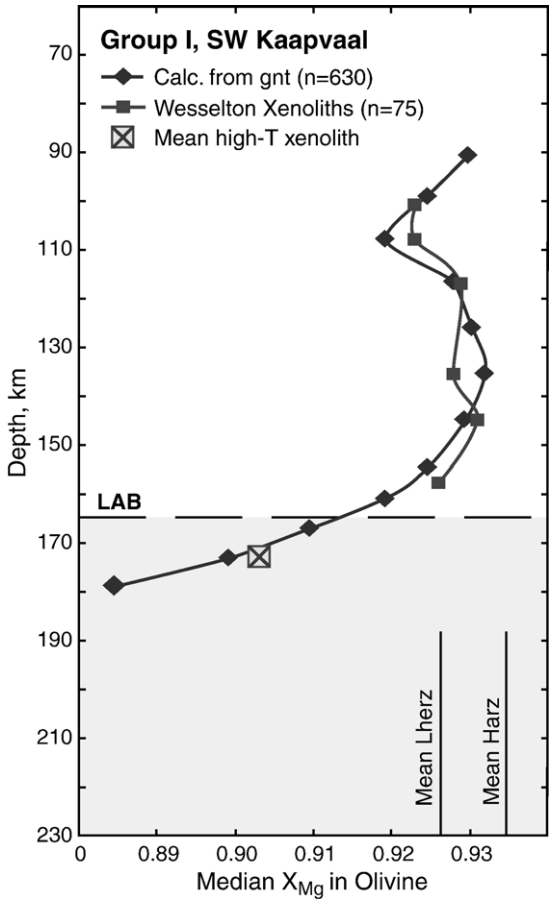

Fig. 6. Variation of olivine composition with depth in the SCLM sampled by Group I kimberlites of the SW Kaapvaal Craton. Diamonds show median values calculated from peridotitic garnets; squares show values measured in a suite of peridotitic xenoliths from one of the kimberlites. Mean values for harzburgites and lherzolites from the same area are shown by vertical lines. The decrease in X_{Mg} toward the LAB is ascribed to metasomatism by small-volume asthenospheric melts; the dip at 100–120 km corresponds to a zone of intense phlogopite-related metasomatism.

towards the base of the lithosphere (Fig. 6; Gaul et al., 2000), which is interpreted as reflecting metasomatic refertilisation of the lower part of the SCLM by (Fe-rich) asthenospheric melts. The uppermost SCLM is commonly characterised by the most Mg-rich (and thus most buoyant) olivine compositions. X_{mg} sections can also reveal layering in olivine composition within the SCLM, providing clues about the nature of both SCLM formation and modification.

2.3. Whole-rock composition: derivation from garnets

To calculate location-specific models of seismic response for the SCLM, we need information on the variation of composition with depth.

Fortunately, much of the petrological context of a garnet xenocryst can be recovered, due to some regular correlations between garnet chemistry and the composition of the host peridotite. In particular, the Cr_2O_3 and Y contents of peridotitic garnets are well correlated with one another, and with whole-rock Al_2O_3 contents, on a global scale (Fig. 7). Increasing whole-rock depletion, as defined by lower Al_2O_3 contents, is reflected in garnets with higher Cr contents and lower Y contents. Griffin et al. (1999b) give an equation for relating Cr^{Gnt} to $Al_2O_3^{WR}$ (Fig. 7). The correlation between the calculated and analysed Al_2O_3 contents for a suite of 133 xenoliths is excellent for values between 1% and 4% Al_2O_3 (Fig. 8). At lower Al contents, the technique tends to slightly overestimate Al; this probably reflects the presence of chromite in many such highly depleted rocks, so that the Cr content in the coexisting garnet does not reflect the true level of depletion.

An alternative approach is to use the Y contents of the garnets, which will be less affected by the presence of chromite, but may be more affected by metasomatic processes. Unfortunately, the number of xenoliths for which both whole-rock analyses and garnet trace-element analyses are available is still small. A relationship bet-

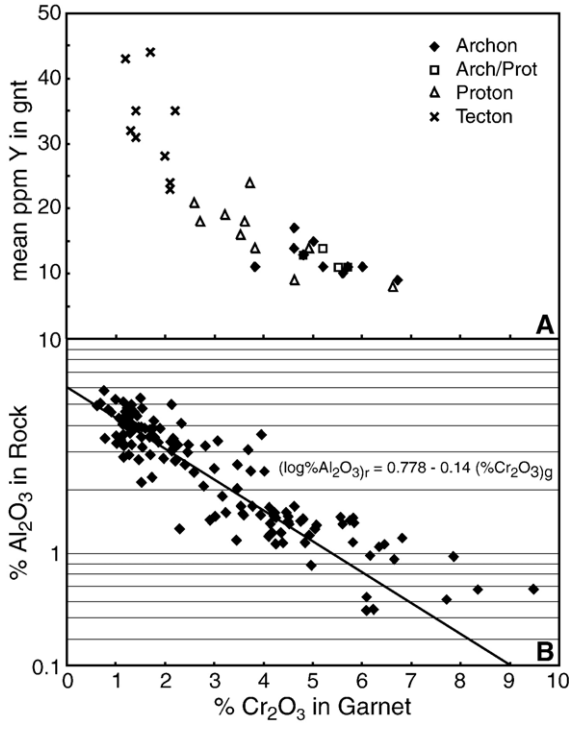

Fig. 7. Correlations among Cr and Y contents of peridotitic garnets and the Al_2O_3 content of host rocks; melt extraction leads to a decrease in whole-rock Al contents, and increases in the Cr and Y contents of garnets. After Griffin et al. (1999a,b,c,d).

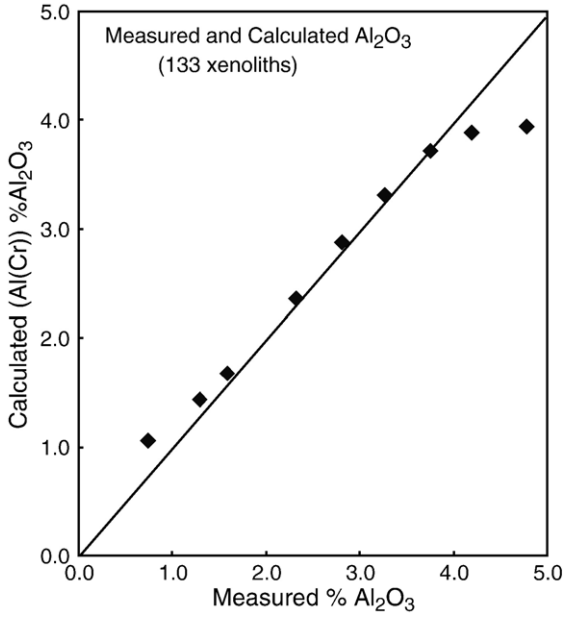

Fig. 8. Correlation between median measured Al_2O_3 contents of peridotite xenoliths and those calculated from the Cr contents of their garnets.

ween Y^{Gnt} and $Al_2O_3^{WR}$ therefore has been derived indirectly, using the Y–Cr relationships in a database of 5000 garnets (Griffin et al., 2002), and is given by: $\%Al_2O_3 = 10\text{^}(0.4515(\ln \text{ppm Y}) - 1.0428)$.

The application of these two approaches to 640 garnets from Group I kimberlites of the Kaapvaal Craton is shown in Fig. 9. At most depths, the curve for Al(Cr) lies up to 0.5 wt.% higher than the curve for Al(Y). Both lie in the range bracketed by the median contents of lherzolite and harzburgite xenoliths from these pipes. The divergence is greatest above 110 km depth, where many xenoliths show coexisting garnet and chromite (Fig. 4d), and the Al(Cr) curve would be expected to overestimate $Al_2O_3^{WR}$.

$Al_2O_3^{WR}$ is a sensitive indicator of depletion through partial melting, as Al is partitioned into the melt phase, leaving the residual mantle depleted in Al. Plots of major oxides against $Al_2O_3^{WR}$ for xenolith suites and massif peridotites (Griffin et al., 1999b) show excellent correlations, which are different between Archean and younger SCLM, and these correlations allow us to calculate the mean composition of the SCLM volumes represented by specific garnet concentrates. Griffin et al. (1999b) have provided algorithms for this purpose and demonstrated excellent agreement between calculated SCLM compositions for specific localities and the mean compositions of xenolith suites from the same areas.

2.4. Calculation of seismic velocity from garnet concentrates

The seismic velocity variation in an SCLM section can be calculated by using measurements of the bulk composition and modal composition of large xenolith suites, combined with experimental data on the elastic parameters of the constituent minerals (e.g. James et al., 2004).

The calculation of density, Vs and Vp profiles for an SCLM section from garnet concentrates requires a series of steps: (1) the calculation of mean bulk compositions for appropriate intervals, as described above; (2) the calculation of a modal mineralogy, by least-squares techniques using the bulk composition and estimated mineral compositions; the X_{Mg} profiles give the composition of the corresponding olivine and the composition of the coexisting orthopyroxene is given by the empirical relationships $X_{Mg}^{Opx} = X_{Mg}^{Ol} + 0.009$ (Archons

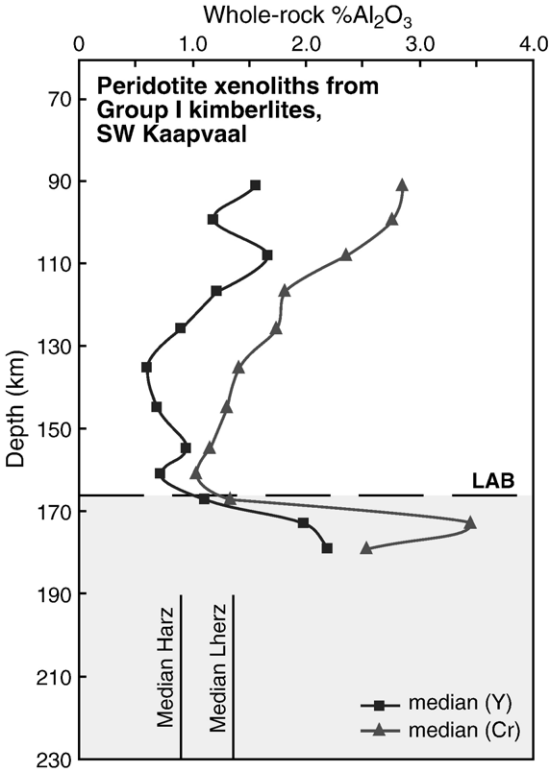

Fig. 9. Depth distribution of median whole-rock Al_2O_3 contents of peridotites, calculated from the Cr and Y contents of garnets from heavy mineral concentrates. The difference between the values calculated by the two methods is greatest through the depth range where chromite is most abundant (Fig. 4c), suggesting that the Al(Cr) curve overestimates the whole-rock Al_2O_3. The sharp increase in Al_2O_3 content at the LAB is attributed to metasomatism by asthenosphere-derived melts.

and Protons) and $X_{Mg}^{Opx} = X_{Mg}^{Ol} + 0.008$ (Tectons), derived from a database of xenolith mineral compositions (authors' unpublished data); the minor, but significant phases clinopyroxene and garnet can be approximated by mean compositions derived from typical Archon, Proton and Tecton samples; (3) the assignment of a temperature and pressure to each interval, using the selected geotherm; (4) an abundance-weighted summation of the elastic parameters of each mineral at the appropriate T and P. Elastic parameters for mantle phases used here are those of Anderson and Isaak (1995). The results for two sections are discussed below. A useful set of algorithms, with a broader and more recent selection of elastic parameters, is provided by Hacker (2003) and Hacker and Aber (2004); these give results essentially identical to those given here.

2.5. Chemical tomography

In this technique, data observables (statistically significant numbers of element abundances in garnets) are inverted to constrain lithospheric rock type distributions.

With the geotherm and a nickel temperature (T_{Ni}) for each garnet grain, the chemical data for a garnet concentrate sample can be plotted against depth (Fig. 2). In many SCLM sections, Y, Zr and Ti tend to vary in similar ways, being removed by the extraction of partial melts, and enriched by subsequent melt-related metasomatism. In other cases, the three elements show strongly decoupled behaviour, which indicates a complex history and carries information on metasomatic processes. The challenge is to examine a large number of variables simultaneously and to recognise the patterns indicative of specific types of process.

Griffin et al. (2002) approached this problem by using three different statistical treatments designed to identify natural populations within a large ($n > 30{,}000$) database of peridotitic garnets analysed for major and trace elements. The most successful approach involved the construction of a parallel "virtual" database, in which the distribution of each variable is identical to that in the natural database, but where no correlations exist among the variables (described in detail in Griffin et al., 2002). The CARP (Cluster Analysis by Regressive Partitioning) technique could then be applied to compare the two databases and divide the compositional space into two types of region: those dominated by real data (13 natural populations) and those dominated by "virtual" data. The results are presented as a simple tree with switches given by values of individual variables (Griffin et al., 2002).

The significance of the individual natural populations was assessed by using the CARP tree to classify the garnets from 210 well-studied xenoliths. 76% of these fall into one of the "natural" populations; those that do not commonly show decoupling of normally correlated elements that suggests complex metasomatic histories (Griffin et al., 2002). The natural populations can be grouped into five broad classes (Fig. 10): subcalcic harzburgites, depleted lherzolites, depleted/metasomatised lherzolites, fertile lherzolites and lherzolites affected by melt-related metasomatism (e.g. the high-T sheared lherzolites common in some kimberlite-borne xenolith suites). The depleted/metasomatised classes show clear evidence, in both trace and major elements,

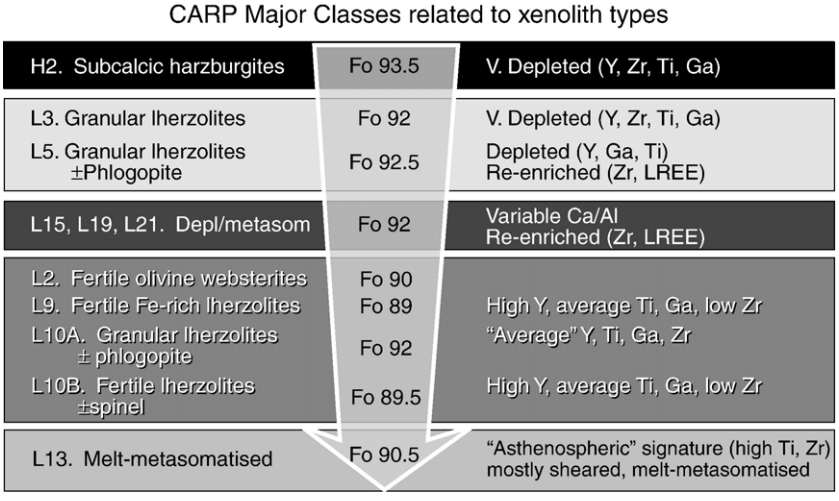

Fig. 10. Summary of the CARP garnet classes used here and their relationship to chemical features of their host peridotites, based on the analysis of >200 well-studied rocks. Arrow illustrates direction of increasing fertility.

of having been originally highly depleted, but later re-enriched by metasomatic activity. The same may be true of some fertile lherzolites with relatively magnesian olivine (class L10A).

The CARP classes thus can be identified with specific processes and lithologies, and their relative proportions in a garnet concentrate can be mapped as a function of depth, to give sections showing the distribution of these processes and rock types. These sections can be combined with profiles of the other important parameters (X_{Mg} in olivine, $Al_2O_3^{WR}$) to construct chemical tomography sections for individual localities (e.g. Fig. 11); these provide the basis for evaluating the geophysical response of the SCLM. These sections show the proportion of specific rock types present at any particular depth slice and give an overall image of the geochemical variation with depth for the lithospheric section sampled by garnets.

2.6. Chemical tomography: examples

2.6.1. Kaapvaal Craton (Group 1 kimberlites)

A section constructed using 640 garnets from 11 Group 1 kimberlites (≤90 Ma old; Smith, 1983) in the SW part of the Kaapvaal Craton is shown in Fig. 11; the geotherm and LAB determination were discussed above (Fig. 4). The LAB at ca. 170 km depth is marked by a large increase in the proportion of melt-metasomatised lherzolites. Depleted harzburgites and lherzolites, and depleted/metasomatised lherzolites, are concentrated in the 130–170 km depth range. Shallower levels are dominated by fertile lherzolites; these are mainly the CARP class L10A, which is typical of phlogopite-bearing lherzolites, and we interpret this fertile zone as reflecting intense metasomatism. The distribution of depleted and fertile rocks is strongly reflected in the X_{Mg} and $Al_2O_3^{WR}$ curves, which also show the large increase in fertility at the LAB.

The calculated profiles for density, Vp and Vs are shown in Fig. 12, and compared with those calculated by James et al. (2004) using a xenolith database ($n=35$). There are strong similarities between the results and most of the discrepancies can be attributed to differences in the relative abundance of some rock types in the garnet and xenolith databases, and the greater depth resolution of the garnet data, stemming from the much larger number of samples. The lower density given by the garnet database in the depth range 120–160 km reflects the higher proportion of harzburgites and depleted lherzolites in the more representative garnet database. This also produces a higher mean Vp, though the Vs calculated by James et al. (2004) in this depth range

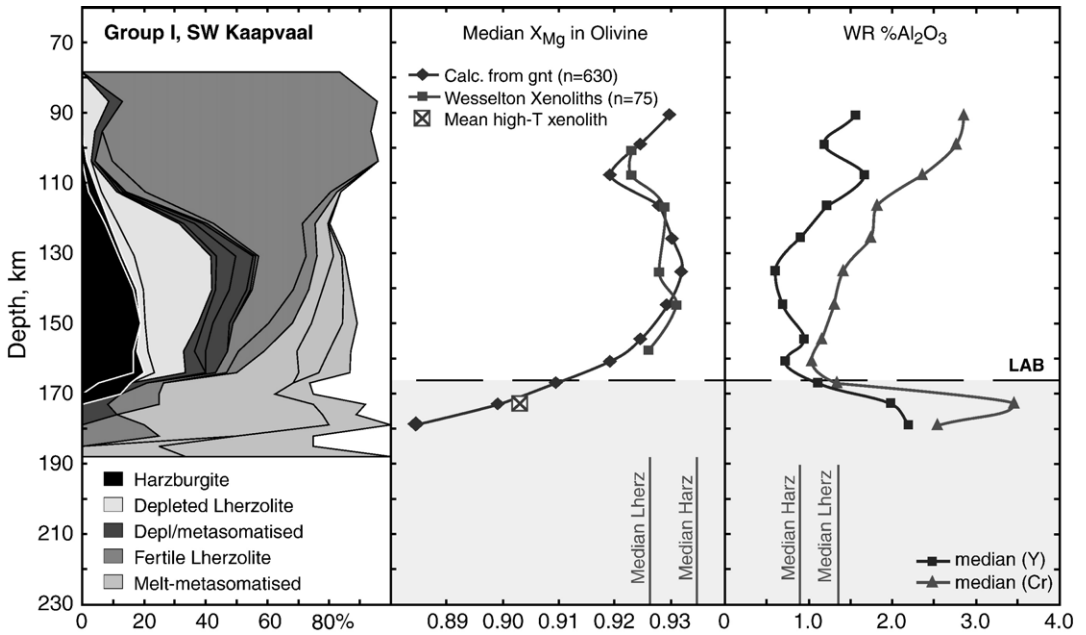

Fig. 11. Chemical tomography section of the SCLM sampled by Group I kimberlites in the SW Kaapvaal Craton, showing the relative abundances of the different CARP groups (Fig. 10) with depth, and their relation to the calculated olivine compositions and whole-rock Al_2O_3 contents. The most magnesian olivine, and the lowest Al_2O_3 contents, correspond to the levels with the highest proportions of harzburgites and depleted lherzolites; the "fertile" lherzolites that dominate above ca. 120 km are the product of metasomatic refertilisation, which has lowered X_{Mg} in olivine and raised whole-rock Al_2O_3.

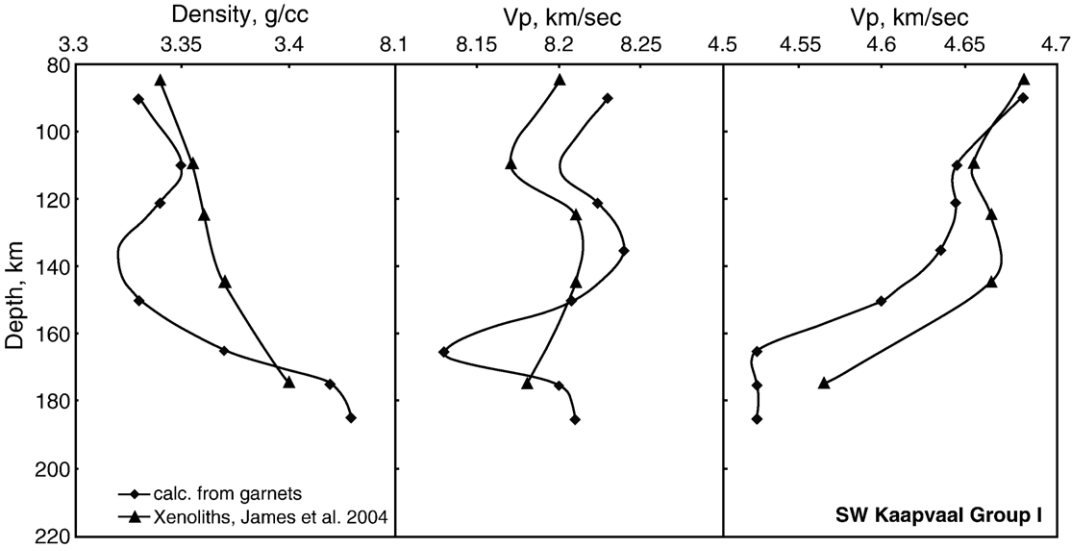

Fig. 12. Variation of density and seismic velocities with depth in the SCLM sampled by the Group I kimberlites of the SW Kaapvaal Craton, as calculated from garnet data (diamonds; this work) and a suite of xenoliths (triangles; James et al., 2004).

is higher than given by the garnet database. Conversely, the somewhat higher mean density, and lower mean Vp, near the LAB (ca. 170 km) reflect the resolution of the garnet database, and the high relative abundance of melt-metasomatised lherzolites at this level, which are undersampled in the xenolith dataset. Both sets of calculations show large vertical variations in Vp and Vs, despite a smooth variation of temperature with depth. However, the only variation that might be sharp enough to register in the seismic signal is the sharp reversal near the LAB, especially in Vp.

2.6.2. Lac de Gras area, Slave Craton

The SCLM beneath the central Lac de Gras sector of the Slave Craton shows a stepped geotherm, rising from a 35 mW/m^2 conductive model to one slightly below the 40 mW/m^2 model at ca. 150 km depth; this implies a possible difference in thermal conductivity above and below this level (Paul Morgan, pers. comm., 2000). This level also coincides with the base of the electrically anomalous layer measured by Jones et al. (2001) as discussed by Poudjom Djomani et al. (2005). The LAB is weakly defined at ca. 190–200 km (Griffin et al., 1999d). The SCLM is strongly layered, with an ultradepleted upper part separated from a more normally depleted portion by a sharp boundary at 145–150 km (Fig. 13); the lower layer also shows a high degree of melt-related metasomatism. The layering is also seen in the X_{Mg} profile; olivine is highly magnesian high in the upper layer and X_{Mg} decreases downward; X_{Mg} drops sharply at the interface and then decreases even more rapidly with depth. Calculations of $Al_2O_3^{WR}$ from Cr and Y contents of garnets differ by 0.5–0.8% in the upper layer, where chromite is ubiquitous (Griffin et al., 1999b), but are very similar in the lower layer, where chromite is less common. The low values of Al(Y) are more likely to be correct and demonstrate the extreme depletion of the upper layer. $Al_2O_3^{WR}$ shows a sharp jump at the top of the lower layer, reflecting a high level of metasomatism there.

The diamonds from the Lac de Gras area are notable for a high proportion of mineral inclusions that were encapsulated in the diamonds at depths >660 km (Davies et al., 1999, 2004). On this basis, we have interpreted the two-layered structure as reflecting the emplacement of a plume head beneath a thin, highly depleted SCLM. Re–Os data on sulfide inclusions in olivine, and whole-rock Re–Os analyses of eclogites from the lower layer, constrain the timing of this event to >3 Ga (Aulbach, 2003; Aulbach et al., 2004).

Calculations of density, Vp and Vs (Fig. 14) show a sharp jump in density at the boundary between the upper and lower layers (ca 150 km); density then decreases with depth to the LAB, where it increases sharply. The layer boundary has little effect on Vp but produces a small drop in Vs; these relatively small effects reflect the partial cancelling of the compositional effects by the rise in the geotherm at the layer boundary. Vp, and especially Vs, decrease markedly with depth through the lower layer and rise again below the LAB. In this case, any "low-velocity zone" would be recorded within the lower part of the lithosphere.

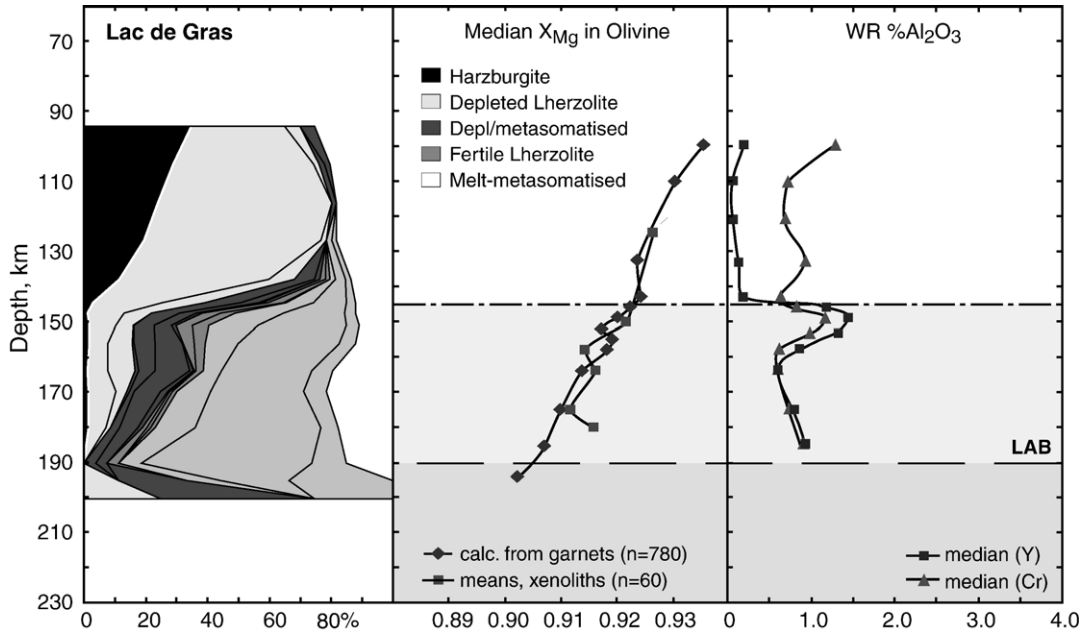

Fig. 13. Chemical tomography section for the Lac de Gras area, central Slave Craton, Canada, showing the ultradepleted upper layer, separated by a sharp boundary at 145 ± 5 km from a more typically Archean (but metasomatised) lower layer, interpreted as a plume head. The X_{Mg} section shows both the olivine compositions calculated from peridotitic garnets and those measured in a suite of xenoliths (Aulbach, 2003). The sharp increase in Al_2O_3 contents at the top of the lower layer is interpreted as due to the accumulation of melts derived from the plume head; it also corresponds to the highest concentration of eclogites (Aulbach, 2003).

Snyder et al. (2003) have analysed receiver-function data from teleseismic stations in the central Slave Craton and recorded a signal from the 150 km discontinuity beneath Lac de Gras, which can be traced across a significant part of the craton. Another signal at ca. 200 km beneath Lac de Gras corresponds to the LAB as mapped by the garnet data. The mantle xenoliths from the Jericho Pipe to the north (Kopylova et al., 1999) reveal that this mantle section has been highly netasomatised along a deep lithosphere discontinuity, a phenomenon not observed in other mantle sections from the Slave Craton. The lithospheric mantle beneath Jericho is therefore anomalous in the larger context of the Slave Craton lithosphere.

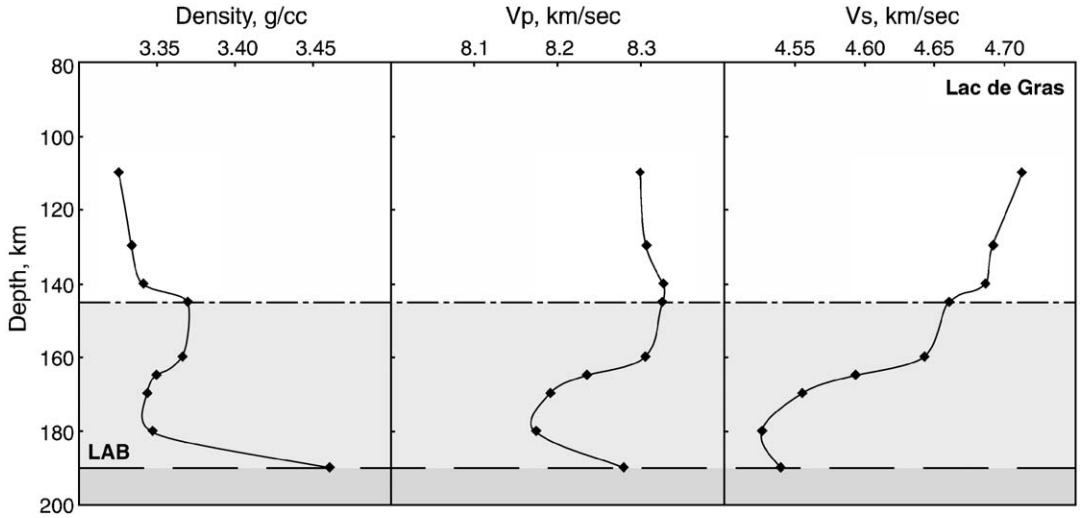

Fig. 14. Variation of density and seismic velocity with depth beneath the Lac de Gras area, calculated from peridotitic garnets; horizontal lines show the position of the boundary between the upper and lower layers, and the LAB.

2.6.3. Colorado Plateau

The Colorado Plateau is a large uplifted area in the SW USA (e.g. Eggler et al., 1988). It is underlain by Proterozoic crust 37–48 km thick (Parsons et al., 1996) and the area has been elevated ca. 2 km since Cretaceous time. Xenoliths and xenocrysts are found in serpentinised ultramafic diatremes and minette plugs. A study of crustal xenoliths by Selverstone et al. (1999) suggests that the boundary between two major Proterozoic terranes, the Yavapai (1.8–2.0 Ga) and the Mazatzal (1.6–1.8 Ga), runs NE–SW through area. There is no evidence in the crustal rocks for an earlier prehistory and the section is shown here as a possible example of juvenile Proton SCLM.

The chemical tomography section (Fig. 15) is dominated by fertile lherzolites; a relatively large proportion of the garnets does not classify in the "real" CARP classes, suggesting complex metasomatic processes (Griffin et al., 2004a and references therein). The overall fertility of the section is reflected in the high values of calculated $Al_2O_3^{WR}$. Chromite are present throughout the section and the Al(Y) values are more consistent with published data for xenoliths from this area. Despite these relatively fertile compositions, X_{Mg} in olivine is high in the upper parts of the section and the mean value is similar to many cratonic localities. This high X_{Mg} would contribute significantly to the buoyancy of the Plateau, which is in isostatic equilibrium (Poudjom Djomani et al., 2001; Griffin et al., 2004a).

2.6.4. Eastern Australia

Eastern Australia is a typical Tecton, developed during Paleozoic to Mesozoic time along the extended margin of the Australian craton. Numerous Tertiary to Quaternary alkali-basalt volcanoes have provided extensive suites of spinel lherzolites, and some localities, such as Jugiong in New South Wales, have provided small garnet lherzolite xenoliths and suites of garnet xenocrysts (Gaul et al., 2003). Similar geotherms have been derived for many localities, using garnet websterite xenoliths (O'Reilly and Griffin, 1985; Xu et al., 1998). Data on analysed spinel peridotites can be projected to these geotherms, providing depth sections that typically are ≤65 km thick.

The xenolith suites from western Victoria show a depleted upper SCLM, with low $Al_2O_3^{WR}$ and relatively high X_{Mg}. Fertility increases downward (Fig. 16). Re–Os studies, using both whole-rock and in-situ (sulfide analysis) techniques, indicate that the depleted rocks are at least Proterozoic (1.8–1.9 Ga) in age (McBride et al., 1996; Handler et al., 1997; Alard et al., 2002), and apparently represent relicts of the cratonic SCLM, preserved during continental extension due to their buoyancy. The more fertile rocks appear to represent Paleozoic to Mesozoic additions to the SCLM. A similar situation has been documented beneath the extended margin of E. China, in the Taiwan Straits (Wang et al., 2003).

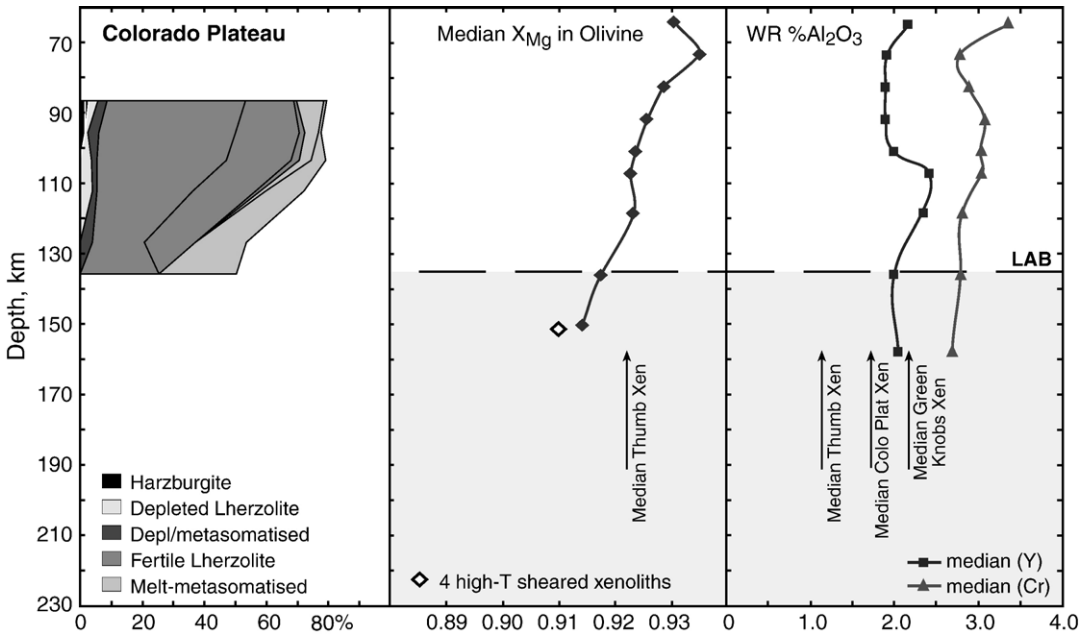

Fig. 15. Chemical tomography section for the Colorado Plateau, with generalised comparative data for xenoliths from The Thumb, Green Knobs and other Colorado Plateau localities.

Mantle sections in north and south Queensland are quite fertile, with no indication of relict SCLM (Fig. 16). This is consistent with their location beneath earlier arc terranes, accreted to the Australian continent late in the Paleozoic orogeny. These would originally have been underlain by the highly depleted mantle typical of arc (and ocean-floor) environments (Griffin et al., 1999b). However, this type of Phanerozoic depleted mantle retains a high Fe content; on cooling, it would have negative buoyancy with respect to the underlying asthenosphere and would tend to delaminate (Poudjom Djomani et al., 2001). This would allow upwelling of the underlying asthenosphere, accompanied by low degrees of partial melting and depletion, to form a new SCLM, only mildly depleted relative to the asthenosphere.

The garnet xenocrysts from Jugiong reflect a deeper, even more fertile SCLM, which is only slightly depleted relative to models for the Primitive Mantle. We also interpret these rocks as upwelling asthenosphere, which has cooled to become part of the SCLM.

3. Secular evolution of SCLM composition

The chemical tomography sections shown here, and from a range of other Archon, Proton and Tecton settings (Griffin et al., 2003, 2004b) illustrate the secular evolution of SCLM composition described in detail by Griffin et al. (1998b, 1999b). Archon SCLM contains rock types that are essentially absent in Proton and Tecton SCLM, such as the subcalcic harzburgites and some classes of highly depleted lherzolites. Proton SCLM contains variable proportions of depleted and depleted/metasomatised lherzolites, and Re–Os data suggest that many of these sections (e.g. northern Botswana; Carlson et al., 1999; Griffin et al., 2004b) may represent Archon SCLM that has persisted through Proterozoic reworking and refertilisation, due to its buoyancy and refractory nature (Poudjom Djomani et al., 2001). Tecton sections, where they represent reworking of older continental volumes, may contain relicts of depleted rocks at shallow depths, as in western Victoria (Fig. 16). However, many Tecton sections consist only of relatively fertile lherzolites, which may represent asthenospheric replacement after delamination of Phanerozoic lithosphere.

This secular evolution is well expressed in a simple plot of CaO^{WR} vs. $Al_2O_3^{WR}$ (Fig. 17). Because fertile SCLM will have significantly lower seismic velocities (Vp, Vs) than depleted SCLM at the same temperature, this secular evolution is important for the interpretation of seismic data.

4. Seismic tomography and SCLM composition

The composition and thermal state of the SCLM beneath North America have been mapped out using garnet concentrates and xenolith data from 28 localities

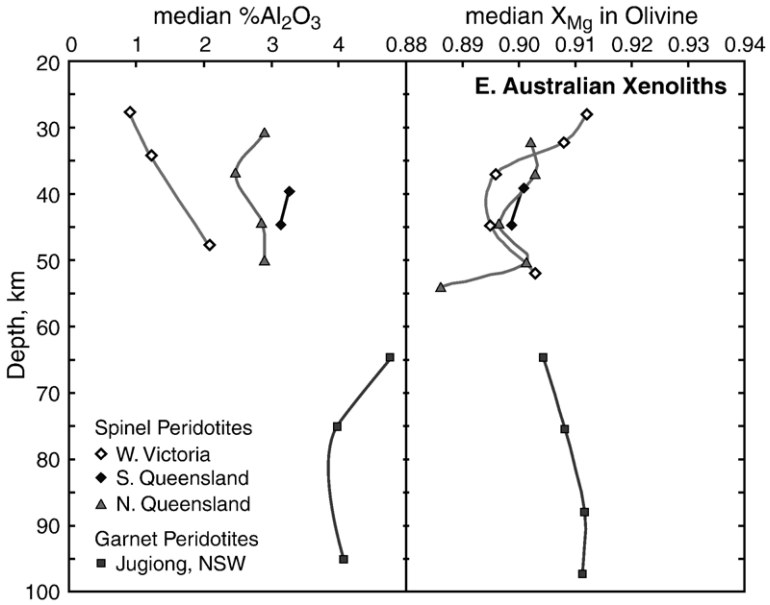

Fig. 16. Variation of median whole-rock Al_2O_3 contents and olivine compositions with depth, measured in spinel peridotite xenoliths from three areas in E. Australia. Values for the Jugiong locality are calculated from peridotitic garnets.

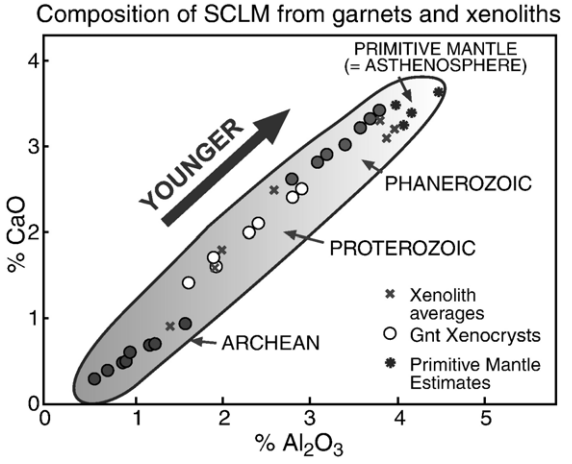

Fig. 17. SCLM compositions calculated from peridotitic garnets and measured as means of xenolith suites, showing the secular evolution of SCLM composition with the tectonothermal age of the overlying crust.

(Fig. 18; Griffin et al., 2004a). These provide a basis for interpreting seismic tomography on the basis of SCLM types. The high-Vs "root" of the continent extends to 200–250 km depth and tapers with depth. There is a good correlation between the thickness of this root and the temperatures at 150 km depth, as determined from the garnet geotherm at each locality. Temperatures ≤1050 °C are confined to the area within the outline of the root, temperatures of 1050–1150 °C occur around its margin, and higher temperatures are found in the Appalachian Tecton and beneath the Colorado Plateau, where the LAB lies at <150 km depth, as discussed above.

Chemical tomography sections for these localities are shown by Griffin et al. (2004a). From the X_{Mg} profiles, we can construct a cross-section along the jagged traverse shown in Fig. 18 and use it to calculate a Vs profile for comparison with the values measured from the tomographic image (Fig. 19). The section shows the thick depleted layer under the Archean Hudson Bay-Michigan region, and how it thins toward the margins of the craton, becoming most fertile beneath the Appalachian Tecton.

Across most of the traverse, in the areas within the outline of the root and with low geotherms, there is good agreement between the observed Vs (100–175 km) and the values calculated using a mean temperature

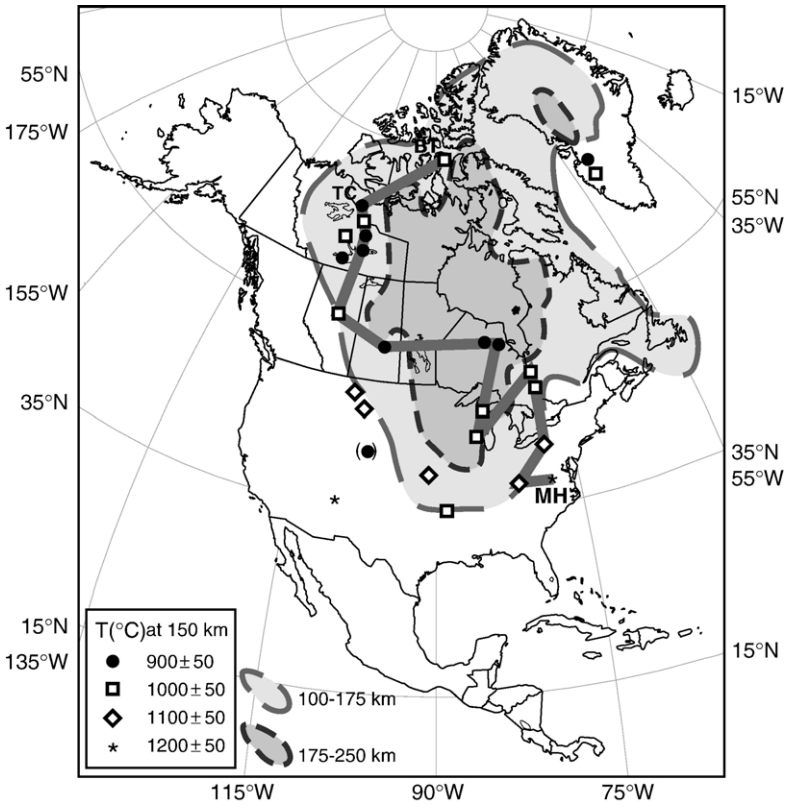

Fig. 18. Map of N. America showing outline of high-Vs root at 100–175 km and 175–250 km (S. Grand, pers. comm., 2003) and temperatures at 150 km depth, derived from garnet geotherms. Dark line shows traverse illustrated in Fig. 19. After Griffin et al. (2004a).

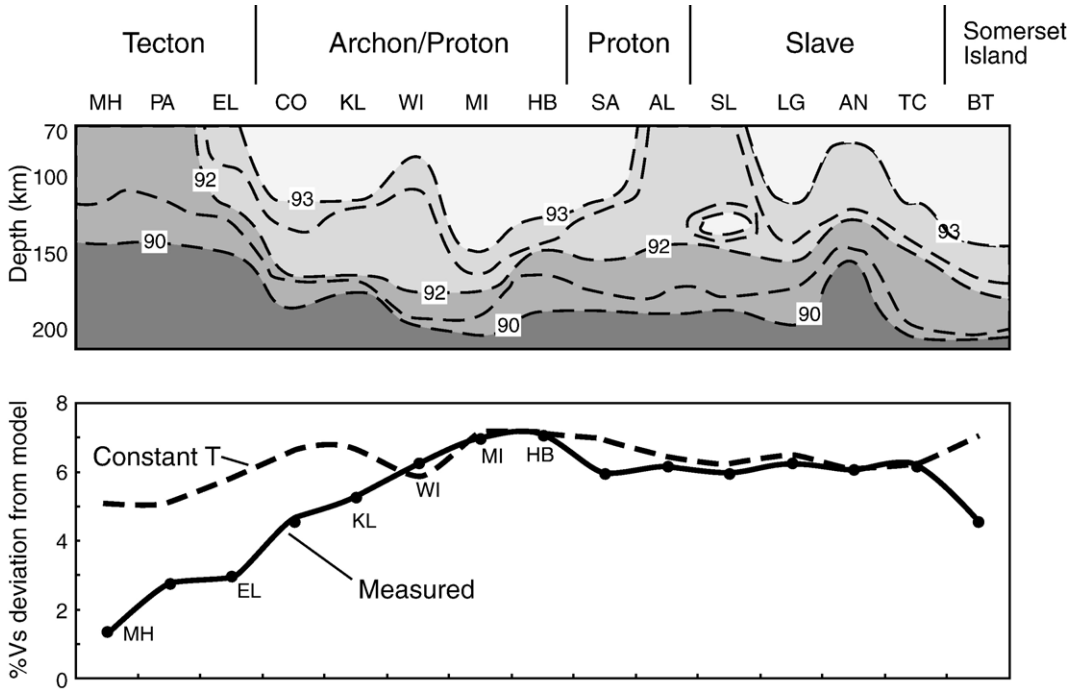

Fig. 19. Top, contours of olivine composition (as %Fo) in the SCLM along the traverse shown in Fig. 18. Bottom, calculated (constant T = 1000 °C) and measured Vs in the 100–175 km depth slice along the traverse. The Vs variation within the main part of the craton is consistent with the compositional variations; deviation of the two curves at the left end reflects the higher geotherms along the eastern margin of the cratonic root. After Griffin et al. (2004a).

of 1000 °C. One exception is the Somerset Island locality, where the thermal effects of the opening of the Arctic Ocean postdate the intrusion of the kimberlites, so that the Vs is lower than predicted by the xenolith and xenocryst data (Schmidberger and Francis, 1999; Griffin et al., 2004a). A similar situation is seen in the Colorado–Wyoming area (Fig. 18), where the Cambrian kimberlites record a low-T and depleted SCLM, which predates Laramide orogenic activity that has raised the geotherm and probably modified the SCLM.

In the craton–margin localities, the constant-T calculation predicts a drop in Vs of ca. 25% relative to the cratonic core, which is much less than is observed. This difference in Vs clearly is caused by the difference in geotherm between the on-craton and off-craton localities. The total drop in Vs from Archon to Tecton thus reflects the cumulative effects of a more fertile SCLM, a thinner SCLM and a rise in temperature.

5. Correlations: the key to seismic interpretation

The observations reviewed here show a series of consistent correlations that are essential to the interpretation of seismic tomography: thick SCLM = depleted SCLM = low geotherm; the depletion and the low geotherm reinforce one another to produce high seismic velocities. Thick SCLM (180–250 km) is typical of Archon areas, but Archon SCLM may persist beneath some Proton areas (e.g. northern Botswana; Griffin et al., 2003). In these cases, the modification of the SCLM toward more fertile compositions will result in lower Vp and Vs even though the geotherm may be similar. Tecton areas generally have the combination of fertile SCLM, thin lithosphere and high geotherm, all of which contribute to low seismic velocity.

These broad correlations are expressed in Fig. 20 by families of X_{Mg} profiles for Archon, Proton and Tecton sections. Most Archon profiles show little variation with depth, before a decrease (sharp or gradual) that marks the LAB. Proton sections show a greater range of variability, probably because some sections represent reworked Archon SCLM (e.g. N. Botswana; Griffin et al., 2003), whereas others (e.g. the Birekte Terrane of N. Siberia; Griffin et al., 1999a) may be juvenile Proterozoic SCLM. They are generally less magnesian, thinner and may have higher geotherms than the Archon sections. Tecton sections also show considerable variability. Most show shallow, fertile sections, with high geotherms. In localities such as Elliott County

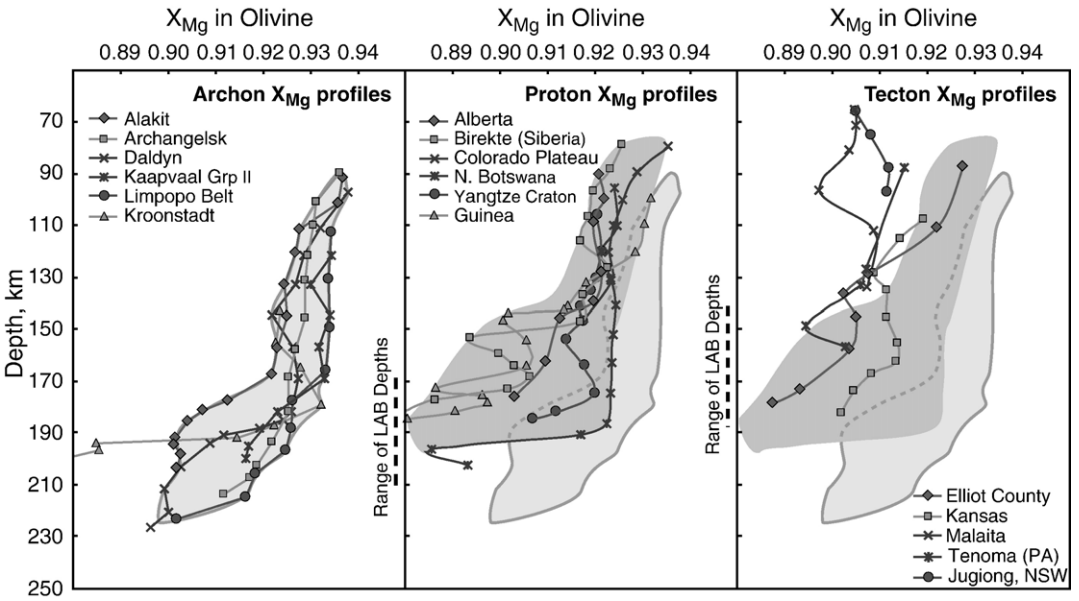

Fig. 20. Families of X_{Mg} profiles for Archon, Proton and Tecton sections worldwide, illustrating the general correlations among tectonothermal age, fertility and SCLM thickness; geotherms also rise with decreasing tectonothermal age (Fig. 5) and these correlations combine to produce the observed rapid lateral changes in Vp and Vs.

and Tenoma, on the edge of the craton (Fig. 18) and Kansas, near the Mid-Continent Rift (Fig. 18), a higher degree of depletion, lower geotherm and deeper LAB probably reflect the persistence of older SCLM.

As noted above, a change of 0.01 in the X_{Mg} of olivine will produce a change of 0.22% in Vs, equivalent to changing T by 90 °C at 100 km depth. However, changes in X_{Mg} do not occur in isolation; X_{Mg} in olivine correlates closely with other indices of fertility and depletion. Thus, the increase in average fertility from Archon to Tecton, reflected in Fig. 20, corresponds to an increase in density of 1.5% and a decrease in Vs of 1.2% (Griffin et al., 2004a) with no change in temperature. The implication of these figures is that SCLM composition must be considered in the interpretation of seismic data.

In principle, there is no unique solution to the question of whether changes in temperature, or changes in composition, are responsible for variations in the seismic signal. Fortunately, as shown here, SCLM fertility, lithosphere thickness and geotherm tend to be strongly correlated, such that each reinforces the effect of the others in raising or lowering seismic velocity. These correlations will produce rapid lateral changes in the seismic properties of the SCLM and are the key to a realistic use of seismic tomography for mapping lithospheric structure. In the future, such interpretations may be significantly improved by using relationships between Vp and Vs, rather than either in isolation.

6. Conclusions

1. Geochemical data from garnet xenocryst suites, ground-truthed against xenolith data where available, can provide high-resolution images of thermal and compositional heterogeneity in the continental lithosphere. These images in turn allow the detailed calculation of geophysical properties for individual SCLM sections and enable the use of geophysical data to extend lithospheric mapping laterally beyond areas sampled by volcanic rocks.
2. The fertility of the SCLM is strongly correlated with its tectonothermal age, as defined by the timing of the last major tectonothermal event in the overlying crust. Archean SCLM is originally highly depleted and variably refertilised; Phanerozoic SCLM is dominantly fertile.
3. Typically, lithosphere thickness is negatively correlated with the tectonothermal age, and hence the fertility, of the SCLM; geotherms show a broad positive correlation with SCLM fertility.
4. The correlated variations in SCLM fertility, lithospheric thickness and geotherm reinforce the effects of each on seismic velocity, and can produce rapid lateral variations in seismic response. It is important to recognise that these seismic variations are not simply due to thermal effects.
5. The preservation of Archean SCLM at shallow levels beneath many areas of younger tectonother-

mal age implies rapid vertical variations in Vs and Vp, and may affect seismic interpretations.

Acknowledgements

We thank Hans Thybo and the organisers of the Copenhagen Workshop for the invitation to present this review. Numerous colleagues (geophysicists and non-geophysicists) have contributed many ideas over more than two decades and, more immediately, Norman Pearson, Paul Morgan, Yvette Poudjom Djomani, Lev Natapov, Graham Begg, Jon Hronsky, Tara Deen, Stephen Grand and Alan Jones have provided insightful input and discussions. This is contribution no. 409 from the National Key Centre for Geochemical Evolution and Metallogeny of Continents (www.es.mq.edu.au/GEMOC).

References

Alard, O., Griffin, W.L., Pearson, N.J., Lorand, J.-P., O'Reilly, S.Y., 2002. New insights into the Re–Os systematics of sub-continental lithospheric mantle from in situ analysis of sulphides. Earth and Planetary Science Letters 203, 651–663.

Anderson, D.L., 1989. Theory of the Earth. Blackwell Scientific Publications, Cambridge, MA. USA. 366 pp.

Anderson, O.L., Isaak, D.G., 1995. Elastic constants of mantle minerals at high temperature. In: Ahrens, T.J. (Ed.), Mineral Physics and Crystallography; A Handbook of Physical Constants. American Geophysical Union, Washington DC, pp. 64–97.

Aulbach, S., 2003. The lithospheric mantle beneath the Slave Craton and Alberta, Canada. Unpubl. PhD thesis, Macquarie University. 262 pp.+Appendices.

Aulbach, S., Griffin, W.L., Pearson, N.J., O'Reilly, S.Y., Doyle, B.J., Kivi, K., 2004. Mantle formation and evolution, Slave Craton: evidence from HSE abundances and Re–Os isotope systematics of sulfide inclusions in mantle xenocrysts. Chemical Geology 208, 61–88.

Birch, F., 1961. The velocity of compressional waves in rocks to 10 kbar, 2. Journal of Geophysical Research 66, 2199–2224.

Bostock, M.G., 1999. Seismic imaging of lithospheric discontinuities and continental evolution. Lithos 48, 1–16.

Carlson, R.W., Pearson, D.G., Boyd, F.R., Shirey, S.B., Irvine, G., Menzies, A.H., Gurney, J.J., 1999. Re–Os systematics of lithospheric peridotites: implications for lithosphere formation and preservation. Proc. 7th Int. Kimberlite Conf.. Red Roof Design, Cape Town, pp. 99–108.

Cull, J.P., O'Reilly, S.Y., Griffin, W.L., 1991. Xenolith geotherms and crustal models in eastern Australia. Tectonophysics 192, 359–366.

Davies, R.M., Griffin, W.L., Pearson, N.J., Andrew, A.S., Doyle, B.J., O'Reilly, S.Y., 1999. Diamonds from the deep: pipe DO-27, Slave Craton, Canada, Proceedings 7th International Kimberlite Conference, Cape Town, vol. 1. Red Roof Design, Cape Town, pp. 148–155.

Davies, R.M., Griffin, W.L., O'Reilly, S.Y., Doyle, B.J., 2004. Geochemical characteristics of diamonds and microdiamonds from kimberlites, Lac de Gras, Slave Craton, Canada. Lithos 77, 99–111.

Eggler, D.H., Meen, J.K., Welt, F., Dudas, F.O., Furlong, K.P., McCallum, M.E., Carlson, R.W., 1988. Tectonomagmatism of the Wyoming Province. Colorado School of Mines Quarterly 83, 25–40.

Finnerty, A.A., Boyd, F.R., 1987. Thermobarometry for garnet peridotite xenoliths: a basis for mantle stratigraphy. In: Nixon, P.H. (Ed.), Mantle Xenoliths. John Wiley and Sons, New York, pp. 381–402.

Gaul, O.F., Griffin, W.L., O'Reilly, S.Y., Pearson, N.J., 2000. Mapping olivine composition in the lithospheric mantle. Earth and Planetary Science Letters 182, 223–235.

Gaul, O., O'Reilly, S.Y., Griffin, W.L., 2003. Lithosphere structure and evolution in southeastern Australia. Special Publication - Geological Society of Australia 22, 179–196.

Griffin, W.L., O'Reilly, S.Y., 1987. Is the Moho the crust–mantle boundary? Geology 15, 241–244.

Griffin, W.L., Ryan, C.G., Cousens, D.C., Sie, S.H., Suter, G.F., 1989. Ni in Cr-pyrope garnets: a new geothermometer. Contributions to Mineralogy and Petrology 103, 199–202.

Griffin, W.L., Smith, D., Ryan, C.G., O'Reilly, S.Y., Win, T.T., 1996. Trace-element zoning in mantle minerals: metasomatism and thermal events in the upper mantle. The Canadian Mineralogist 34, 1179–1193.

Griffin, W.L., Zhang, A., O'Reilly, S.Y., Ryan, C.G., 1998a. Phanerozoic evolution of the lithosphere beneath the Sino-Korean craton. In: Flower, M.F.J., Chung, S.-L., Lo, C.-H., Lee, T.-Y. (Eds.), Mantle Dynamics and Plate Interactions in East Asia. Geodynamics Series. American Geophysical Union, pp. 107–126.

Griffin, W.L., O'Reilly, S.Y., Ryan, C.G., Gaul, O., Ionov, D.A., 1998b. Secular variation in the composition of subcontinental lithospheric mantle. In: Braun, J., Dooley, J.C., Goleby, B.R., van der Hilst, R.D., Klootwijk, C.T. (Eds.), Structure and Evolution of the Australian Continent, Geodynamics, vol. 26. Amer. Geophys. Union, Washington D.C., pp. 1–26.

Griffin, W.L., Ryan, C.G., Kaminsky, F.V., O'Reilly, S.Y., Natapov, L.M., Win, T.T., Kinny, P.D., Ilupin, I.P., 1999a. The Siberian lithosphere traverse: mantle terranes and the assembly of the Siberian craton. Tectonophysics 310, 1–35.

Griffin, W.L., O'Reilly, S.Y., Ryan, C.G., 1999b. The composition and origin of sub-continental lithospheric mantle. In: Fei, Y., Bertka, C.M., Mysen, B.O. (Eds.), Mantle Petrology: Field Observations and High-pressure Experimentation: A Tribute to Francis R. (Joe) Boyd, The Geochemical Society, Special Publication, vol. 6, pp. 13–43.

Griffin, W.L., Fisher, N.I., Friedman, J., Ryan, C.G., O'Reilly, S.Y., 1999c. Cr-pyrope garnets in the lithospheric mantle: I. Compositional systematics and relations to tectonic setting. Journal of Petrology 40, 679–704.

Griffin, W.L., Doyle, B.J., Ryan, C.G., Pearson, N.J., O'Reilly, S.Y., Davies, R., Kivi, K., van Achterberg, E., 1999d. Layered mantle lithosphere in the Lac de Gras area, Slave Craton: composition, structure and origin. Journal of Petrology 40, 705–727.

Griffin, W.L., Fisher, N.I., Friedman, J.H., O'Reilly, S.Y., Ryan, C.G., 2002. Cr-pyrope garnets in the lithospheric mantle: II. Compositional populations and their distribution in time and space. Geochemistry, Geophysics, Geosystems, #1073 3 (12) (35 pp).

Griffin, W.L., O'Reilly, S.Y., Natapov, L.M., Ryan, C.G., 2003. The evolution of lithospheric mantle beneath the Kalahari Craton and its margins. Lithos 71, 215–241.

Griffin, W.L., O'Reilly, S.Y., Doyle, B.J., Pearson, N.J., Kivi, K., Malkovets, V., Coopersmith, H., Pokhilenko, N.V., 2004a. Lithosphere mapping beneath the North American plate. Lithos 77, 873–922.

Griffin, W.L., Graham, S., O'Reilly, S.Y., Pearson, N.J., 2004b. Lithosphere evolution beneath the Kaapvaal Craton: Re–Os systematics of sulfides in mantle-derived peridotites. Chemical Geology 208, 89–118.

Gung, Y., Panning, M., Romanowicz, B., 2003. Global anisotropy and the thickness of continents. Nature 422 (6933), 707–711.

Hacker, B.R., 2003. Subduction factory: 1. Theoretical mineralogy, densities, seismic wave speeds, and H_2O contents. Journal of Geophysical Research 108 (B1), 2029, doi:10.1029/2001JB001127.

Hacker, B.R., Aber, G.A., 2004. Subduction factory: 3. An excel worksheet and macro for calculating the densities, seismic wave speeds, and H_2O contents of minerals and rocks at pressure and temperature. Geochemistry, Geophysics, Geosystems, doi:10.1029/2003GC000614.

Handler, M.R., Bennett, V.C., Esat, T.M., 1997. The persistence of off-cratonic lithospheric mantle: Os isotopic systematics of variably metasomatised southeast Australian xenoliths. Earth and Planetary Science Letters 151, 61–75.

Helmstaedt, H.H., Gurney, J.J., 1995. Geotectonic controls of primary diamond deposits: implications for area selection. Journal of Geochemical Exploration 53, 125–144.

Ito, E., Kubo, T., Katsura, T., Walter, M.J., 2004. Melting experiments of mantle materials under lower mantle conditions with implications for magma ocean differentiation. Physics of the Earth and Planetary Interiors 143–144, 397–406.

James, D.E., Boyd, F.R., Schutt, D., Bell, D.R., Carlson, R.W., 2004. Xenolith constraints on seismic velocities in the upper mantle beneath southern Africa. Geochemistry, Geophysics, Geosystems 5 (1), Q01002, doi:10.1029/2003GC000551.

Janse, A.J.A., 1994. Is Clifford's Rule still valid? Affirmative examples from around the world. In: Meyer, H.O.A., Leonardos, O. (Eds.), Diamonds: Characterization, Genesis and Exploration. Dept. Nacional da Prod. Mineral, Brazilia, pp. 215–235.

Jones, A.G., Ferguson, I.J., Chave, A.D., Evans, R.L., McNeice, G.W., 2001. Electric lithosphere of the Slave Craton. Geology 29, 423–426.

Kopylova, M.G., Russell, J.K., Cookenboo, H., 1999. Petrology of peridotite and pyroxenite xenoliths from the Jericho kimberlite: implications for the thermal state of the mantle beneath the Slave Craton, northern Canada. Journal of Petrology 40 (1), 79–104.

McBride, J.S., Lambert, D.D., Greig, A., Nicholls, I.A., 1996. Multistage evolution of Australian subcontinental mantle: Re–Os isotopic constraints from Victorian mantle xenoliths. Geology 24, 631–634.

McEnroe, S.A., Langenhorst, F., Robinson, P., Bromiley, G.D., Shaw, C.J., 2004. What is magnetic in the lower crust? Earth and Planetary Science Letters 226, 175–192.

McKenzie, D., Bickle, M.J., 1988. The volume and composition of melt generated by extension of the lithosphere. Journal of Petrology 29, 625–679.

Menzies, M.A., 1990. Petrology and geochemistry of the continental mantle: an historical perspective. In: Menzies, M.A. (Ed.), Continental Mantle. Oxford University Press, Oxford, UK, pp. 31–43.

Nyblade, A.A., 1999. Heat flow and the structure of Precambrian lithosphere. Lithos 48, 81–91.

O'Neill, H.S.C., Wood, B.J., 1979. An experimental study of Fe–Mg partitioning between garnet and olivine and its calibration as a geothermometer. Contributions to Mineralogy and Petrology 70, 59–70.

O'Reilly, S.Y., Griffin, W.L., 1985. A xenolith-derived geotherm for southeastern Australia and its geophysical implications. Tectonophysics 111, 41–63.

O'Reilly, S.Y., Griffin, W.L., 1996. 4-D lithospheric mapping: a review of the methodology with examples. Tectonophysics 262, 3–18.

O'Reilly, S.Y., Griffin, W.L., Gaul, O., 1997. Paleogeothermal gradients in Australia: key to 4-D lithosphere mapping. AGSO Journal of Australian Geology and Geophysics Centenary 17, 63–72.

O'Reilly, S.Y., Griffin, W.L., Poudjom Djomani, Y.H., Morgan, P., 2001. Are lithospheres forever? Tracking changes in subcontinental lithospheric mantle through time. GSA Today 11, 4–10.

Parsons, T, et al., 1996. Crustal structure of the Colorado Plateau, Arizona: application of new long-offset seismic data analysis techniques. Journal of Geophysical Research 101 (B5), 11173–11194.

Pavlenkova, N.I., 1997. General features of the upper mantle structure from seismic data. In: Fuchs, K. (Ed.), Upper Mantle Heterogeneities from Active and Passive Seismology. Kluwer Academic Publishers, The Netherlands, pp. 225–236.

Pollack, H.N., Chapman, D.S., 1977. On the regional variation of heat flow, geotherms and lithospheric thickness. Tectonophysics 38, 279–296.

Poudjom Djomani, Y.H., O'Reilly, S.Y., Griffin, W.L., Morgan, P., 2001. The density structure of subcontinental lithosphere through time. Earth and Planetary Science Letters 184, 605–621.

Poudjom Djomani, Y.H., O'Reilly, S.Y., Griffin, W.L., Natapov, L.M., Erinchek, Y., Hronsky, J., 2003. Upper mantle structure beneath eastern Siberia: evidence from gravity modeling and mantle petrology. Geochemistry, Geophysics, Geosystems 4 (7), 1066, doi:10.1029/2002GC000429.

Poudjom Djomani, Y.H., O'Reilly, S.Y., Griffin, W.L., 2005. Variations of the elastic thickness (Te) and structure of the lithosphere beneath the Slave Province, Canada. ASEG 35, 266–271.

Robinson, P., Harrison, R.J., McEnroe, S.A., Hargraves, R.B., 2002. Lamellar magnetism in the haematite–ilmenite series as an explanation for strong remanent magnetization. Nature 418, 517–520.

Ryan, C.G., Griffin, W.L., Pearson, N.J., 1996. Garnet geotherms: a technique for derivation of P–T data from Cr-pyrope garnets. Journal of Geophysical Research 101 (B3), 5611–5625.

Schmidberger, S.S., Francis, D., 1999. Nature of the mantle roots beneath the North American craton: mantle xenolith evidence from Somerset Island kimberlites. Lithos 48, 195–216.

Selverstone, J., Pun, A., Condie, K.C., 1999. Xenolithic evidence for Proterozoic crustal evolution beneath the Colorado Plateau. Geological Society of America Bulletin 111 (4), 590–606.

Smith, C.B., 1983. Pb, Sr and Nb isotopic evidence for sources of southern African Cretaceous kimberlites. Nature 304, 51–54.

Smith, D., 1999. Temperatures and pressures of mineral equilibration in peridotite xenoliths: review, discussion and implications. In: Fei, F., Bertka, C.M., Mysen, B.O. (Eds.), Mantle Petrology: Field Observations and High Pressure Experimentation: A Tribute to Francis R. (Joe) Boyd, The Geochemical Society, pp. 171–188.

Snyder, D.B., Rondenay, S., Bostock, M.G., Lockhart, G.D., 2003. Mapping the mantle lithosphere for diamond potential. Ext. Abst. 8th International Kimberlite Conf., Victoria. (unpaged).

Snyder, D.B., Rondenay, S., Bostock, M.G., Lockhart, G.D., 2004. Mapping the mantle lithosphere for diamond potential using teleseismic methods. Lithos 77, 859–872.

Thybo, H., 2002. Deep seismic probing of the continents and their margins. Tectonophysics 355, 1–5.

Wang, K.-L., O'Reilly, S.Y., Griffin, W.L., Chung, S.-L., Pearson, N.J., 2003. Proterozoic mantle lithosphere beneath the extended margin of the South China Block: in situ Re–Os evidence. Geology 31, 709–712.

Wyllie, P.J., 1988. The origin of kimberlite. Journal of Geophysical Research 85, 6902–6910.

Xu, X., O'Reilly, S.Y., Griffin, W.L., Zhou, X., 1996. A xenolith-derived geotherm and the crust–mantle boundary at Qilin, southeast China. Lithos 38, 41–62.

Xu, X., O'Reilly, S.Y., Griffin, W.L., Zhou, X., 1998. The nature of the Cenozoic lithosphere at Nushan, eastern China. In: Flower, M., Chung, S.L., Lo, C.H., Lee, T.Y. (Eds.), Mantle Dynamics and Plate Interactions in East Asia, Geodynamics Series, vol. 27. Amer. Geophys. Union, Washington D.C., pp. 167–196.